Anisotropy is Everywhere, to See, to Measure, and to Model

Nick Barton
NB&A, Fjordveien 65c, Høvik, Oslo, 1363 Norway,
nickrbarton@hotmail.com

Eda Quadros
BGTech, Rua Miguel de Almeida Prado 20, Butantá, São Paulo, Brazil,

ABSTRACT: Anisotropy is everywhere. Isotropy is rare. Round stones are collectors' items, and any almost cubic blocks are photographed, as they are the exception.The reasons for rock masses to frequently exhibit impressive degrees of anisotropy, with properties varying with direction of observation and measurement, are clearly their varied geological origins. Origins may provide distinctive bedding cycles in sedimentary rocks, distinctive flows and flow-tops in basalts, foliation in gneisses, schistosity in schists and cleavage in slates, and faults through all the above. We can add igneous dykes, sills, weathered horizons, and dominant joint sets. *Each* of the above are rich potential or inevitable sources of velocity, modulus, strength and permeability anisotropy – and inhomogeneity. The historic and present-day stress anisotropy provides a wealth of effects concerning the preferentially oriented jointing, with its reduced roughness and greater continuity. High stress may also have induced oriented micro-cracks. All the above reinforce disbelief in the elastic-isotropic-continuum or intact-medium-based assumptions promoted by commercial software companies and used by so many for modelling rock masses. RQD and Q are frequently anisotropic as well, and Q is anisotropic not just because of RQD. The authors therefore question whether the *a priori* assumption of homogeneous-isotropic-elastic behaviour has any *significant* place in the scientific practice of realistic rock mechanics

KEYWORDS: Anisotropy, anisotropic structure, stress, velocity, modulus, permeability.

1 INTRODUCTION

In a great range of applications stretching from tectonophysicists' interest in anisotropically distributed microcracks, civil engineers' concerns with low modulus dam foundations, petroleum engineers' interest in the anisotropic permeability of fractured reservoirs, and tunnelling engineers' concerns with the approaching fault zone, the common ocurrence of anisotropy, and inhomogeneity, and its detection with seismic measurements, actually unites many fields of earth science. Anisotropy affects a host of important properties, which will be the subject of this review paper. However, in a temporary lighter vein, why do we find only a few completely round pebbles or boulders ? Why do we seldom find almost cubic blocks which could be their primary source at the base of a sea-cliff or far up a river valley? How many mountain screes have almost cubic-shaped rock debris? When we find the above they are 'collectibles' or at least may be photographed as unusual features. Yet we are 'constantly' modelling in rock mechanics and rock engineering as if isotropy and homogeneity were the rule rather than the exception.

Beside *intrinsic* geologic-origin anisotropy, there is (an often related) stress anisotropy. The two combined, result in a host of *state variable* anisotropic behavioural trends, including the effect of stress-aligned microcracks on the' intact' rock E-moduli, and the effects of anisotropically distributed jointing causing anisotropic rock mass deformation moduli, anisotropic permeabilities, and anisotropic seismic velocities. A large body of velocity data is reviewed in Barton (2006), with emphasis on the typical anisotropic velocity signatures. Some of this seismic anisotropy data will be reviewed later, because velocities varying with directions of measurement is a particularly clear illustration of the dangers of assuming isotropic properties.

Conveniently for the earth sciences, seismic, sonic or ultra-sonic investigations can be applied over a virtually unlimited range of scales. It is the anisotropic response that is the richer though more complex signal source. The earth and its response to changes (excavation, dam loading, water supply, petroleum supply) are usually *anisotropic*: they are not usually *isotropic*. However, microcracked samples and jointed rock masses are particularly sensitive to the degree of saturation, since they are seismically much more visible when dry and unloaded, than when saturated and strongly loaded. This of course is a source of difficulty. Nevertheless, shear-wave polarization into fast and slow axes, due to even faint anisotropy, remains as the evidence of potential fractured reservoirs, if another source of anisotropy is also present: a cap rock with higher minimum stress than the shear-stress (differential-stress) resisting reservoir rock.

Even in the presently unstressed state in a laboratory, and even if stresses are isotropic, the presence of microcracks, fabric, bedding or jointing will give anisotropic distributions of seismic velocity if these features are themselves anisotropically distributed, as is obviously the case for fabric and sedimentary structures. Micro-cracks that are closed by stress give higher velocity in the direction of the applied stress. Fabric such as schistocity will also give velocities that are strongly dependent on stress levels, when the loading is normal to fabric and the rock is dry. The same reasoning applies to joint sets which are closed by the stress or depth effect. When however loading is parallel to predominant microcracks, fabric or jointing, parallel velocities are usually higher than those perpendicular, and there is less sensitivity to stress level, either in the dry or saturated states in this parallel-to-loading direction.

2 THE APPEARANCE OF ANISOTROPY

A pictorial introduction to this paper is appropriate, because the appearance of rock masses is strongly dependent on their degrees of anisotropy. This in turn sets the scene for the investigation and testing strategy, and how best to present, and model, and interpret, the measured anisotropic properties.

A most fundamental property of the majority of the rock masses exposed at the earth's surface is that they are bedded. Beds are in layers and obviously may have varied properties (Figure 1a). When a bedded sequence is also sheared and clay-bearing, as in the example from Kashmir (Figure 1b), the anisotropic properties have been accentuated. Consider the *anisotropic stress, shear strength, deformation modulus, velocity, permeability (ASSSDMVP).*In the case of the slate-like grits from Aberystwyth, western Wales, the cleavage is crossed by a single (anisotropic) clay-free minor fault. A 15 m long wave-cut 'tunnel' is the remarkable final result of these two intersecting anisotropic features. The tunnel will continue to increase in size during the next millennia. The clay-filled dominant joint set illustrated in Figure 1d guarantees the anisotropy of almost all (ASSSDMVP) properties.

Cooling joints in columnar basalt illustrated in Figures 2a and 2c, which will be sub-vertical if the original terrain was horizontal, of course represent an ultimate example of anisotropy, in particular the extremely low normal stiffness of the columns, and corresponding ultra-high axial permeability. Cross-hole velocity measurements within an exploratory drift at the Hanford basalt site in the USA (King et al., 1984) shown in Figure 2b demonstrated a 1.5 to 2.0 km/s velocity

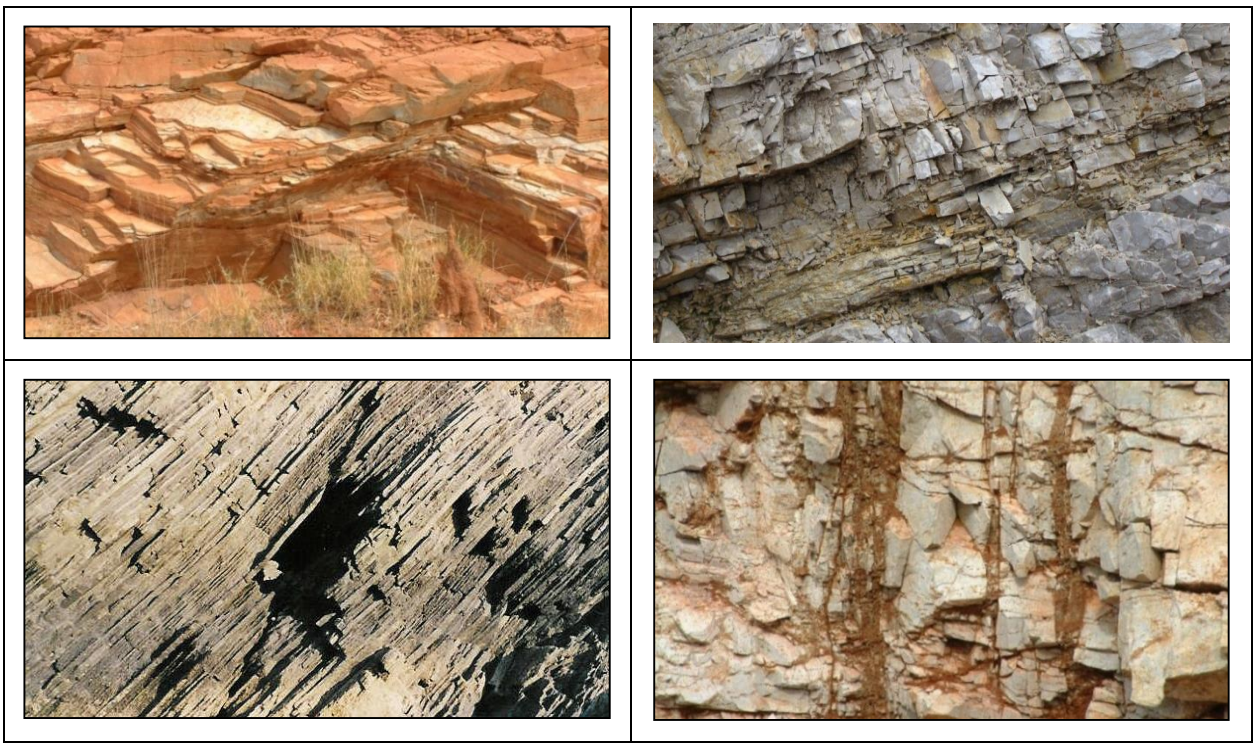

Fig 1a to 1d Sandstone from the Melbourne area, sheared and clay-bearing sandstones and siltstones from Kashmir, slate-like grits from Aberystwyth, western Wales, hornfels with clay-fillings from Asker, southern Norway

anisotropy when testing parallel or perpendicular to the columns, and there was a significant reduction in horizontal velocity ($V_{p\text{-horiz}}$) next to a free face. If permeability anisotropy was measured it would involve many orders of magnitude differences between K_h and K_v. Instead of $V_{p\text{-horiz}} < V_{p\text{-vert}}$ we would then see $K_v >> K_h$. Dominant joint sets, and through-cutting, or cross-cutting fault zones are obviously the ultimate anisotropic features, which will cause many engineering challenges in tunnelling and at dam sites. Some examples are shown in Figures 3a to 3c. Tunnelling may be stopped frequently, and faults sometimes consist of running clay, or conduct huge quantities of water on one side of their clay 'core'. Clearly these are continuous highly anisotropic features, particularly in relation to the directional shear strength. The minor fault showing extreme planarity is of course a highly anisotropic structure, in particular regarding shear and normal stiffness (1:100 ?) and shear strength. Presently sub-vertical bedding in limestones in the Zagros mountains in Iran, represents the weakness direction that has allowed extensive folding to occur in highly stressed conditions in the geologic past.

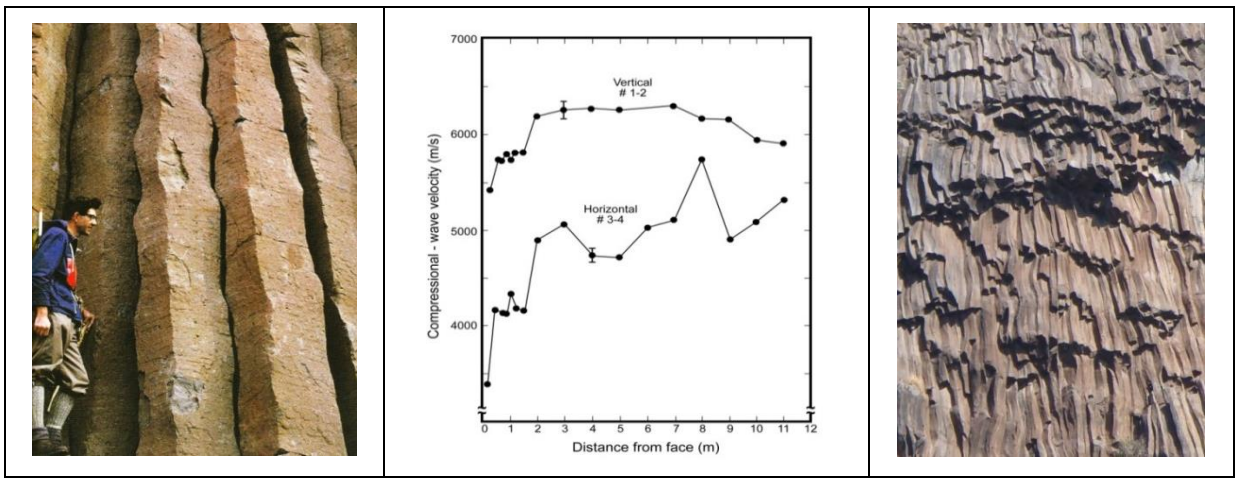

Fig 2a to 2c Columnar basalt with its sub-vertical hexagonal cooling joints, is a classic example of anisotropic deformability, velocity and permeability. Because of its proneness to loosening next to an excavation, the horizontal velocity is reduced, thereby demonstrating an excavated disturbed zone (EDZ)

Fig 3a to 3c Examples of anisotropic features which were obviously exploited by tectonic shearing and/or folding, thereby developing more extreme anisotropy, as found at present day dam sites. The examples are from Iran (Bakhtiary, Zagros) and the bedding-parallel fault is from India (Nathpa Jakri). Figure 4 shows the remarkable Zagros deformations

Fig 4 Exploitation of anisotropic weakness due to bedding, in subsequent kink-bands and folding. The Zagros mountains are known to be the result of almost 20% shortening of the limestone strata. Photograph downstream of Bakhtiary 315 m high arch dam in Iran

3 MODULI, STRESS, STRENGTH, PETROLEUM

This unusual section heading is given to focus attention on an economic winner for all who benefit from petroleum reserves, even though this might be the main source of our climate-change problems in the future. The two contrasting cases to be described, firstly concern the effect of differences in *deformation moduli* created by anisotropy (and inhomogeneity) in the case of inter-bedded sedimentary rocks. In the near-surface this creates some significant differences in the *minimum stress*, which are reflected in logical differences in K_0. Mini-frac stress measurements were conducted by the first author at up to a few hundreds of meters depth, and the location of the boreholes in relation to the sedimentary units are illustrated in Figure 5. The results of shut-in pressures

giving minimum stress levels, showed lowest K_0 (σ_h / σ_v) for shale (0.44-0.52), with increases through siltstone (0.70-0.87), to the highest K_0 in sandstone (1.19-1.63).

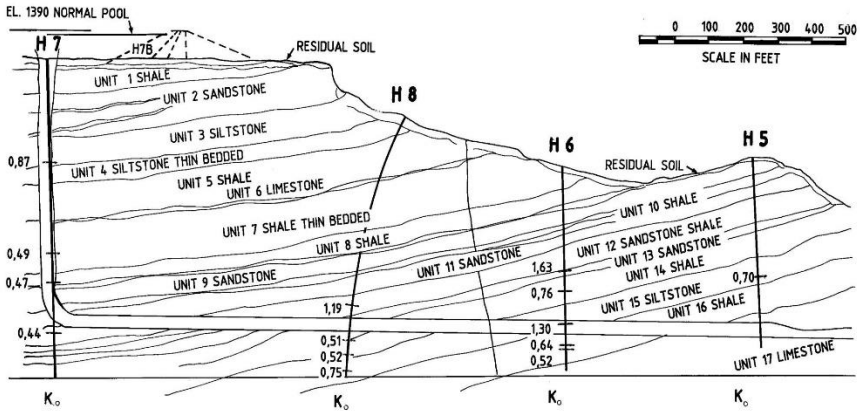

Fig 5 Hydraulic-fracturing (mini-frac) stress measurements in a bedded sequence at the Rock Mountain pumped storage project, Georgia, USA. Values of $k_0 = \sigma_h/\sigma_v$ are shown. (Barton, 1981)

Fortunately for the world's petroleum reserves, past and present, the *weakness* of shale (and salt rock) cap-rocks, and the *strength* of sandstones and carbonates (and producible gas-shales), causes this *K_0 logic* to be reversed at depth, as significant stress differences cannot be tolerated by weak cap-rocks at several kilometers depths. This reversal is illustrated in Figure 6. The high K_0 of shale and salt at depth, due to their *low shear strength*, and the lower K_0 of reservoir rocks due to their *higher shear strength*, gives a form of reversed anisotropy with increased depth.

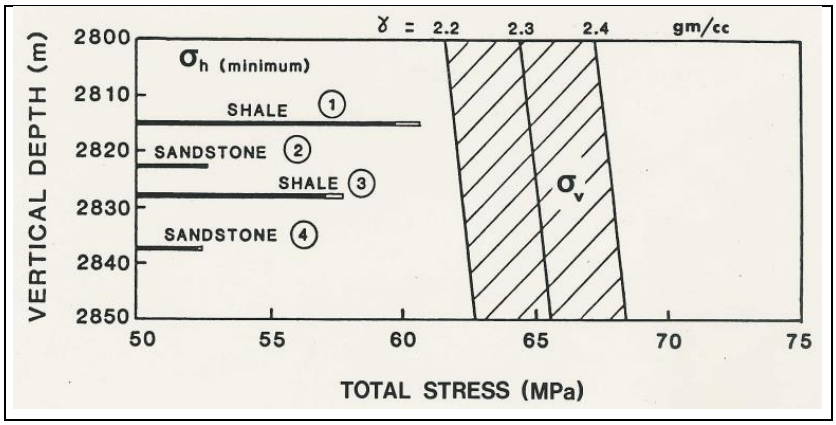

Fig 6 Reversed stress anisotropy is measured at several kilometers depth (Barton, 1986), because the shale or salt caprocks (and clay-bearing fault-seals), cannot tolerate shear stress, while the reservoir rocks can

It is therefore that we have petroleum reserves, but when this satisfactory seal mechanism has not been found, the seabed (if offshore), has characteristic signs of long-term leakage. In the case of gas-shales, the producing shales need to be stronger than the containment layers, which do the same job, and also limit hydro-fracking growth.

4 EFFECTS OF HISTORIC STRESS ANISOTROPY ON JOINTING

An interesting feature of stress anisotropy *history* on joint set development, is that the *surface roughness* of different joint sets (described by for instance Jr or JRC) *increases* as stress anisotropy has itself *declined*. The most planar and smoothest joints with lowest JRC (excluding bedding) were formed when stress anisotropy was high. Figure 7 illustrates the contrast of joint planarity in the 'N-S' direction (with lowest JRC_n = 1, and Jr = 1 as examples), and the significantly higher roughnesses in subsequently fractured directions, when stress anisotropy is expected to have been less.

Stress anisotropy also affects joint apertures in the hydraulically connected or partially connected network of jointing. Since frequency, aperture, and roughness are also affected by anisotropic stresses, the permeability of rock masses becomes potentially highly anisotropic. This will be the subject of a later section. This hydraulic parameter varies by orders of magnitude, due to both historic and present-day stress anisotropy.

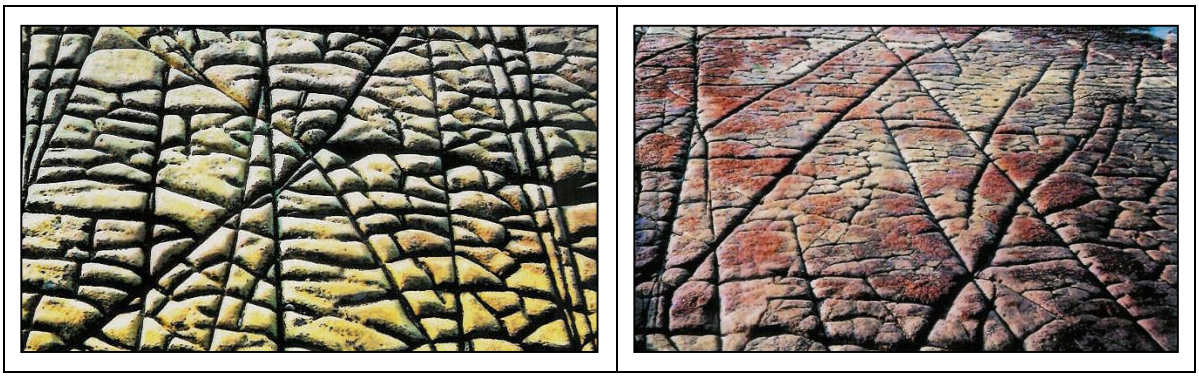

Fig 7 Wave-cut dolomite layers in Kimmeridge Bay shales, showing strong signs of prior stress anisotropy

The sheared and dilated tension fracture replicas shown in Figure 8a have $JRC_0 \approx 20$, and promote the highest permeability anisotropy – but only if they become sheared. Block-size in the context of shearing is given by the mean spacing of cross-joints, i.e. crossing the joints in question.

Observing the roughness profiles reproduced in Figure 8, we could suggest that the shear strength anisotropy of a rock mass with one set of joints of given roughness, and the stiffness anisotropy (Kn/Ks) of the joints in question, will both be maximised by the lower JRC (and lower Jr) magnitudes. The rougher joints maximise permeability anisotropy because of their roughness-enhanced dilation, and the effect on the 'cubic' flow relationship, assuming shear stresses were high enough to get such rough joints mobilized in shear.

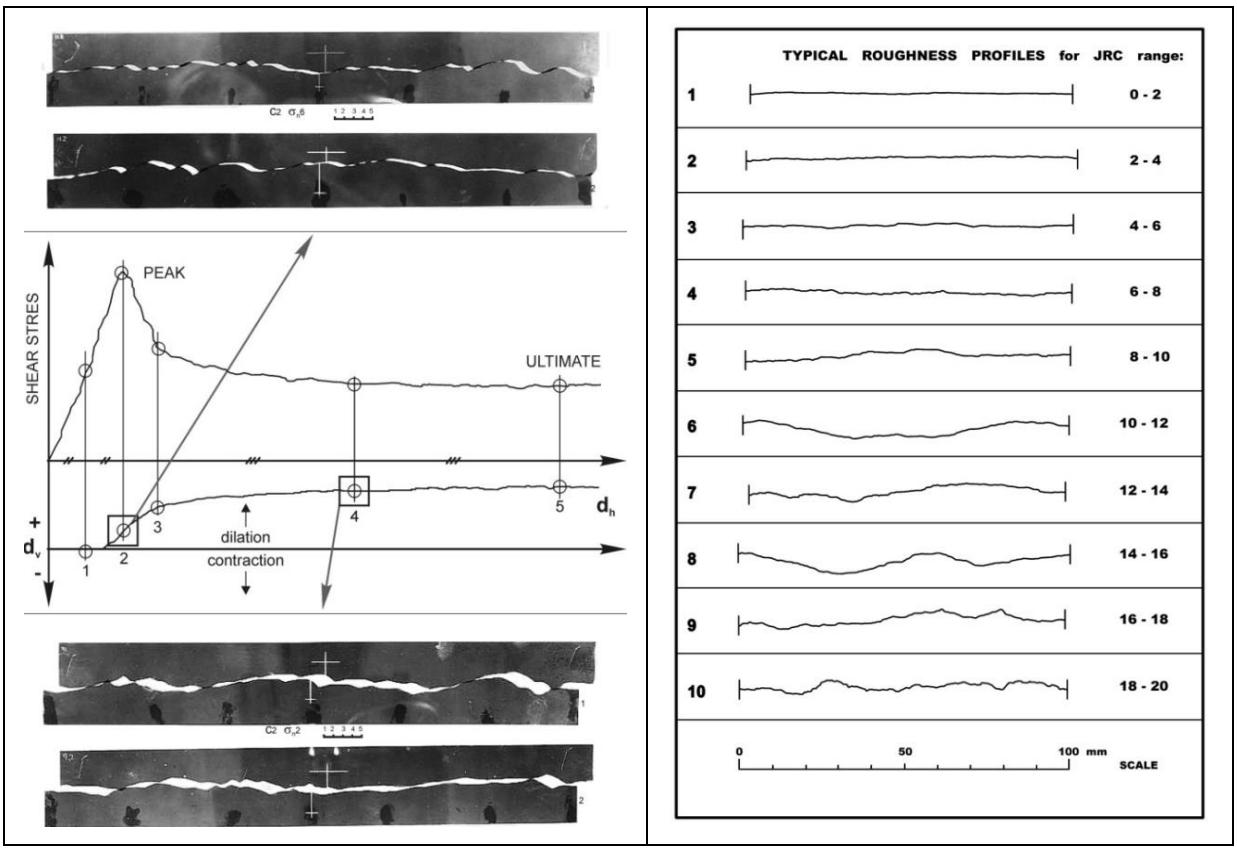

Fig 8a and b Shearing and dilation promote huge potential increases in permeability anisotropy. (Barton, 1973). Standard laboratory-scale (100 mm) JRC_0 roughness profiles from Barton and Choubey (1977). With block-size increase, the JRC_n values are somewhat reduced due to scale effects

5 JOINTING INDUCED ANISOTROPY

The presence of bedding partings, tension fractures, joints, and faults, represents an anisotropic 'mechanism' ready to be mobilized (or re-mobilized) at different scales. Since shear stiffness (Ks) is of so much smaller magnitude than normal stiffness Kn (with Kn/Ks ≈ 1:50, or even 1:100), it is inevitable that the very presence of jointing (of whatever roughness) is an automatic cause of deformation- and especially strength-anisotropy. Continuum modelling of situations where dominant joint set orientations are actually present is inevitably a gross approximation, and is bound to give incorrect results. Most of the assumptions involved are *a priori* in nature (not based on experience). These include the assumptions of linear elastic or bi-linearly elasto-plastic, homogeneous, and isotropic behaviour. Nevertheless when there is a low level of loading and strain, these simplifying assumptions have to be accepted as a first step.

Clearly, a joint will eventually resist further joint closure. If either of these two 'anisotropy mechanisms' are activated, by slope formation or dam loading, we may see shear-dilation-permeability coupling, or closure-permeability coupling that can easily dwarf the natural permeability anisotropies (to be described later). An exaggerated example of this can be visualized from Figure 8a, which was created from correctly sheared and correctly dilated tension fractures (with JRC ≈ 20). Post-peak dilations create potentially huge permeability anisotropy (and inhomogeneity), even when joint roughness is much less. The latter makes shearing more likely, so the phenomenon is self-propagating.

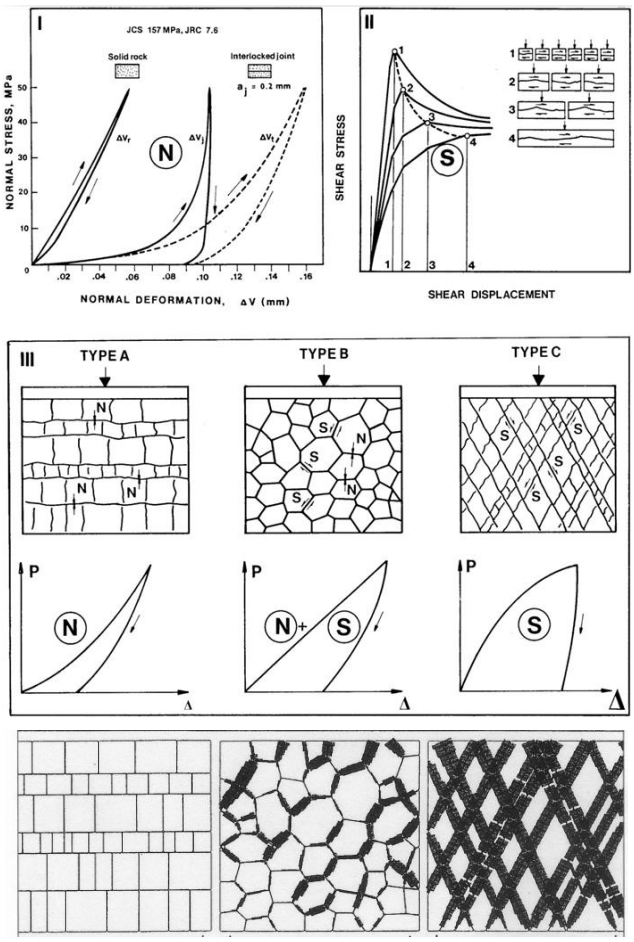

Fig 9a to c Top: Normal and shear components N and S superimposed on Bandis et al. (1981) and (1983) results. Centre: N or S dominated 'rock mass' behaviour as a result of idealized uniaxial loading. Bottom: The UDEC-BB numerical modelling exposes where jointed (DEM) modelling will be essential due to the

strongly anisotropic response. Barton, (1986)

If we examine the three basic rock mass structures (idealized in Figure 9), we see that even uniaxial loading (P) may promote anisotropic (or conjugate) response if there are joint sets present which may be sheared. In the case of the 'basalt'(imagining it loaded perpendicularly to sub-vertical columns as at an arch dam site), normal and shear components 'cancel', and linearity and pseudo-isotropy is maintained. However, if biaxial and also *unequal stress* was applied as a boundary condition, even (A) the 'sedimentary rock' example, would behave anisotropically, due to bed shearing. The first writer was involved in a pumped-hydro project in Taiwan, where thirteen bedding planes crossing the large power cavern were effectively clay-bearing fault zones, needing clay replacement by concrete in the arch, and specially (doubly-) inclined anchors in the walls, so as to limit shearing in this highly anisotropic sedimentary rock mass. In this case the bedding faults were dipping at about 35°in relation to the (assumed) vertical and horizontal principal stresses. (Barton, 1994).

6 THREE-DIMENSIONAL PERMEABILITY ANISOTROPY

The UDEC-BB non-linear modelling of 'jointed rock mass' deformation modes shown in the bottom of the last figure (Figure 9c) is of course a strong demonstration of how there could be significant changes of permeability as a result of the shearing shown by the 'black' lines. However, the modelling of the pre-shear-closure starting state could also mean strong permeability anisotropy. In the case of the 'sedimentary' rock depicted on the left of Figure 9c, one could have the situation that bedding-plane joints were the most permeable. If instead they were clay-sealed or healed, it would be the vertical joints with dominant flow potential. Of course the beds themselves in the case of sandstones, could give strongest permeability anisotropy if the porosity pore-spaces were well connected. Figures 10a and 10b represent examples where permeability anisotropy could be several orders of magnitude, with one case dominated by vertical permeability, and the other case dominated by horizontal permeability.

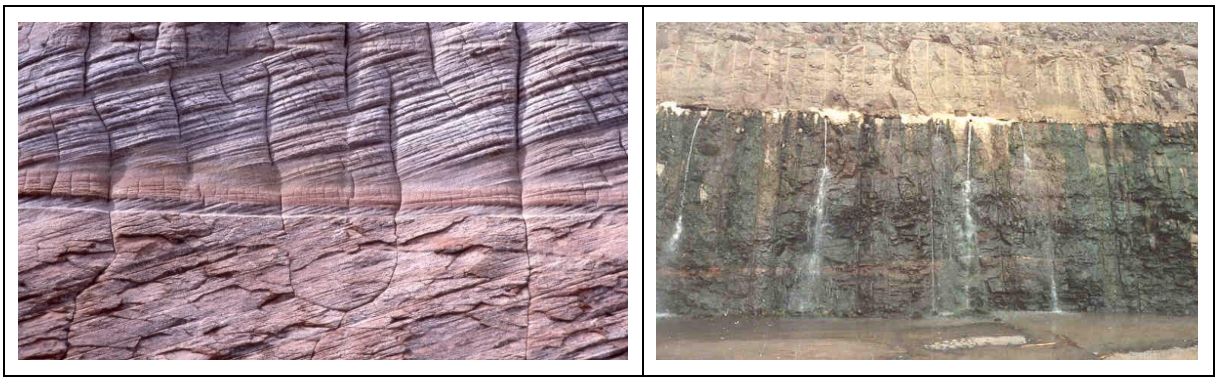

Fig 10a and b Contrasting examples of marked permeability anisotropy. Left: vertical joints dominate in sandstones. This may be related with a previous dominant vertical stress (Zion National Park, USA). Right: A gapped and weathered flow-top in basalts causes huge permeability anisotropy (and grouting challenges). The equivalent conducting aperture was ≈ 2 mm. Quadros and Abrahão (2002)

In situ measurements of the three-dimensional permeability at dam sites and at metro projects in rock (Quadros and Correa Filho, 1999, Quadros and Abrahão, 2002), showed evidence of strong permeability anisotropy. When the rock mass was grouted, permeability tensors were found to have rotated and reduced in magnitude. The three-dimensional testing principle illustrated in Figure 11 was used to investigate possible scale-effects (suitable REV) at the Porta Primavera Dam site in Brazil. Boreholes were drilled in equilateral triangular patterns, with 5m, 15m and 40m spacing, from the common apex hole A. Pump-out from one hole at a time, one packered section at a time, and monitoring of pressures in all other packered sections of the neighbouring holes, was the test principle used.

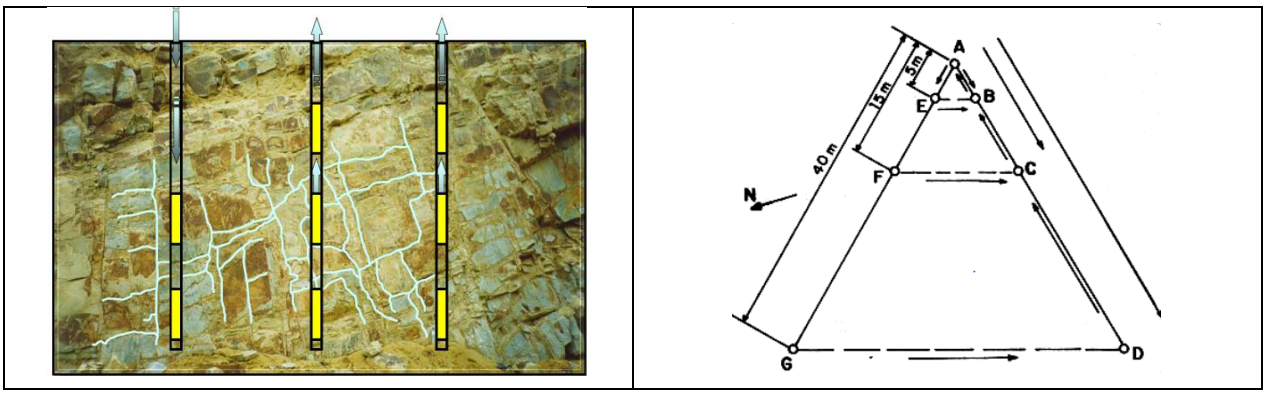

Fig 11a and b Three-dimensional permeability testing using, in this case, three holes at once, with multiple cross-hole pressure reduction monitoring due to pumping out from successive packered sections of each borehole in turn (Quadros and Correa Filho, 1999)

The results of the 3D testing at different scales is shown in Figure 11c. For the three different scales of measurement, the Eigenvalues (principal permeability tensor components) are shown, in units of cm/s. High conductivity is indicated together with significant anisotropy ratios. The latter do not reduce with increased scale of measurement, suggesting that in this case, more conductive joints are involved as the scale is increased. An REV has clearly not been reached, which perhaps is symptomatic in river valleys with some larger scale structures.

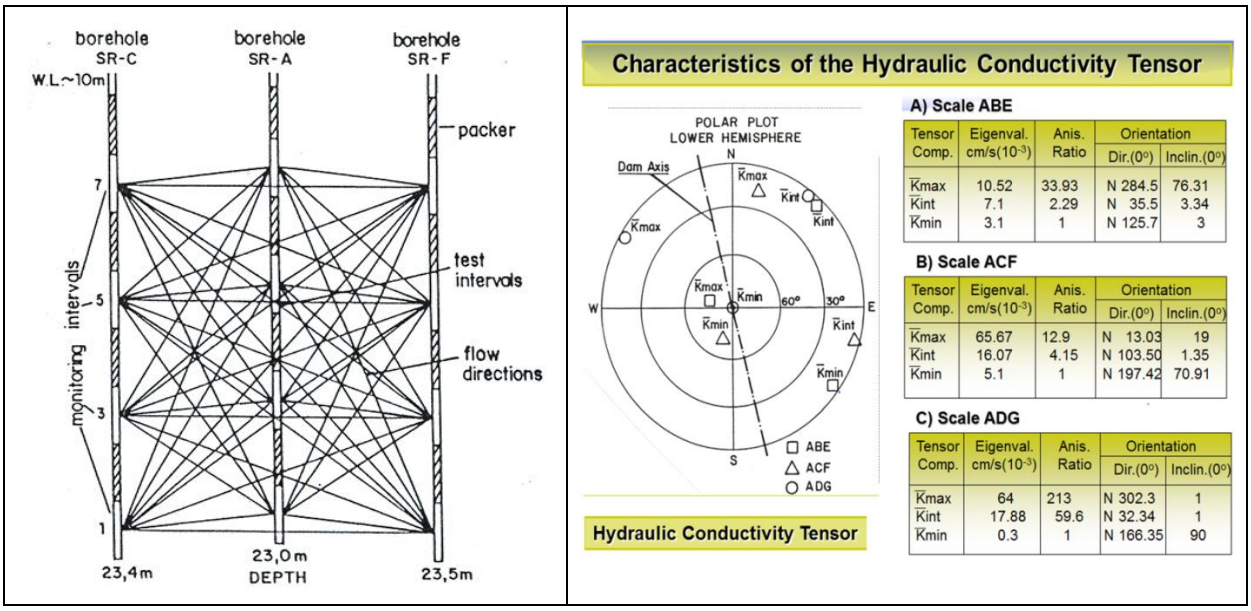

Tensor Comp.	Eigenval. cm/s(10^{-3})	Anis. Ratio	Orientation Dir.(0°)	Orientation Inclin.(0°)
$\bar{K}max$	10.52	33.93	N 284.5	76.31
$\bar{K}int$	7.1	2.29	N 35.5	3.34
$\bar{K}min$	3.1	1	N 125.7	3

Tensor Comp.	Eigenval. cm/s(10^{-3})	Anis. Ratio	Orientation Dir.(0°)	Orientation Inclin.(0°)
$\bar{K}max$	65.67	12.9	N 13.03	19
$\bar{K}int$	16.07	4.15	N 103.50	1.35
$\bar{K}min$	5.1	1	N 197.42	70.91

Tensor Comp.	Eigenval. cm/s(10^{-3})	Anis. Ratio	Orientation Dir.(0°)	Orientation Inclin.(0°)
$\bar{K}max$	64	213	N 302.3	1
$\bar{K}int$	17.88	59.6	N 32.34	1
$\bar{K}min$	0.3	1	N 166.35	90

Fig 11 c and d Hydraulic conductivity tensors obtained by the hydrotomographic test method, with holes in a triangular 3D pattern with 5, 15 or 40 m spacing between holes. Porto Primavera Dam. (Quadros and Correa Filho, 1993)

Due to sampling of a more permeable feature somewhere within the larger 40 x 40 x 40 m triangular measurement dimension, *increased* permeability anisotropy was demonstrated at the largest scale. Note also the 'mixture' of K_{max}, $K_{int,}$ and K_{min} in some of the polar positions. Principal orientations swing around considerably, which of course adds to the challenge of representation in (e.g.) DFN discrete fracture models like FRACMAN or NAPSAC. Note that K_{max}/K_{min} = 213 at the largest scale of measurement. (Quadros & Correa Filho, 1993).

Figure 12 is a compact summary of another set of uncommon field tests from Brazil, which indicate that three-dimensional testing using multiple boreholes can help to prove what has been gained by successful (or unsuccessful) grouting. In these particular before-and-after-grouting 3D water permeability tests, which were performed in a permeable dam abutment, the preliminary, conventional interpretation of individual borehole tests showed reductions of permeability from 1 to 4 orders of magnitude (i.e. from 10^{-7} to 10^{-8} m/s, or from 10^{-5} to 10^{-7} m/s, or from 10^{-4} to 10^{-8} m/s).

In a three dimensional sense, the three principal permeability tensors all rotated as a result of the grouting, signifying good or partial sealing of at least three sets of joints. The reductions in K_{max} and K_{min} were more than one order of magnitude (despite the 6 to 8 m, widely separated boreholes). In addition, despite use of industrial cement and bentonite at that time, the anisotropic rock mass was greatly improved, with the most permeable set presumably sealed first, in a typical anisotropic 'pressure-plateau' response, which is seen when performing high-pressure pre-injection ahead of tunnels, due presumably to successive hydraulic opening of the differently stressed (and variable permeability) joint sets. All the above are indications of anisotropic behaviour involving both permeability and stress.

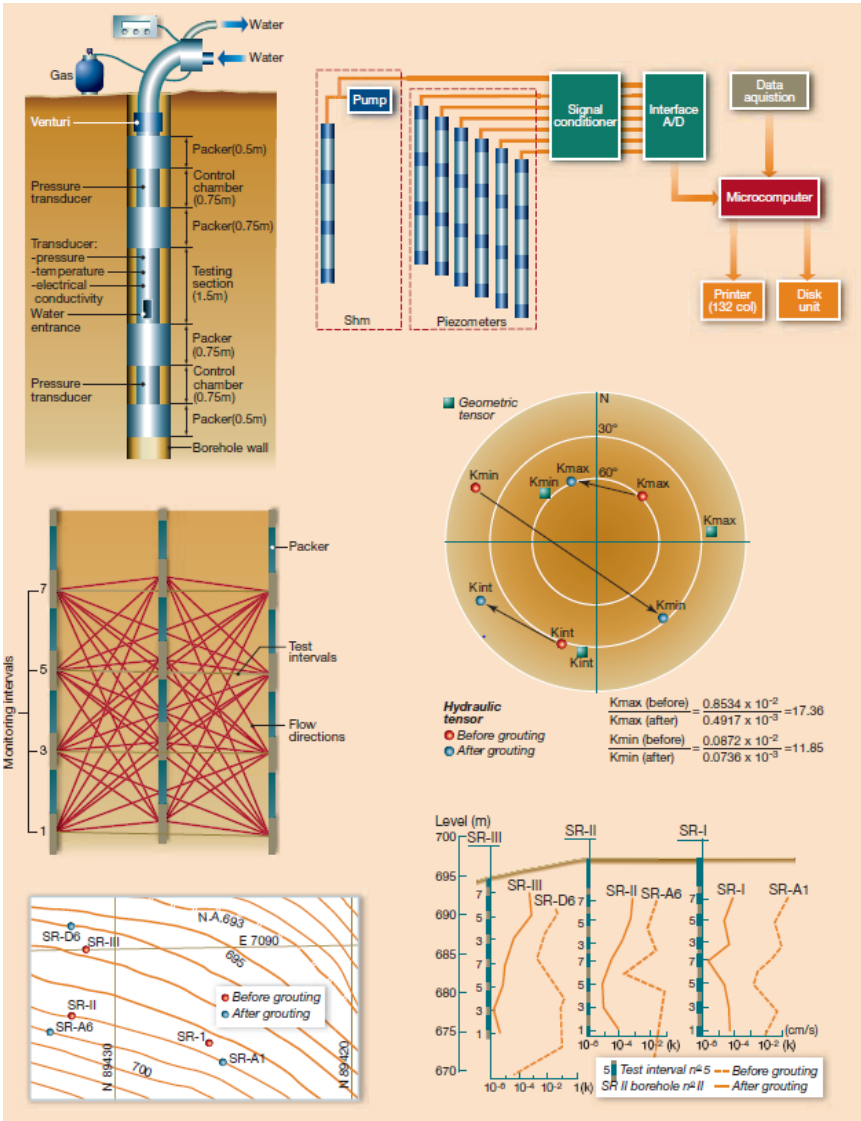

Characteristics of the hydraulic conductivity tensor before cement grouting

TENSOR COMPONENTS	EINGENVALUES (x 10 $^{-2}$ cm/s)	ANISOTROPY RELATIONS	ATITUDE	
			STRIKE (degrees)	DIP (degrees)
K_{max}	0.8534	9.79	N 46.13	57.34
K_{int}	0.1912	2.19	N 197.86	29.44
K_{min}	0.0872	1	N 295.26	12.85

Characteristics of the hydraulic conductivity tensor after cement grouting

TENSOR COMPONENTS	EINGENVALUES (x 10 $^{-2}$ cm/s)	ANISOTROPY RELATIONS	ATITUDE	
			STRIKE (degrees)	DIP (degrees)
K_{max}	0.4917	6.68	N 339.68	58.75
K_{int}	0.2157	2.93	N 240.68	5.43
K_{min}	0.0736	1	N 147.45	30.67

Fig 12 Three-dimensional permeability testing performed between three boreholes, both before and after grouting, showed rotation and reduction in magnitude of the eigenvalues (principal permeability components), and greatly increased bulk modulus. (Quadros and Correa Filho, 1998)

7 SEISMIC ANISOTROPY

The transmission of P and S waves through rock specimens, and through shallow rock masses as a result of refraction seismic measurements, gives rock mechanics and rock engineers a mostly clear indication of anisotropic properties. Although small dynamic strains are involved with the passage of seismic waves, there is nevertheless a subtle response from the non-linear components, via normal and shear compliances (the inverse of dynamic stiffnesses), and more attenuation is experienced (loss of energy per wave cycle) in the more deformable near-surface rock masses, which might include frequency-dependent so-called ‘squirt losses’ in the case of partial saturation. This means fluid movement from micrcracks to pores and vice versa.

In a wide reaching literature survey ranging from lab-scale rock physics experiments to in situ well-monitoring near active faults, it was found that the commonly used ‘seismic quality’ (= 1/attenuation) used by geophysicists, had magnitudes very similar to the (static) rock mass deformation moduli E_{mass} used in rock engineering, *when the latter were expressed in GPa*. A range for $Q_{p\ seismic}$ from 5 to 150 was extremely common (Barton, 2006). Some key examples of seismic anisotropy from this literature survey are given in this section of the paper. We progress from micro-cracks, through schistocity and cleavage, to sedimentary layering and finally to the effect of jointing in larger-scale VSP surveys. Refer to Figures 13 through 17.

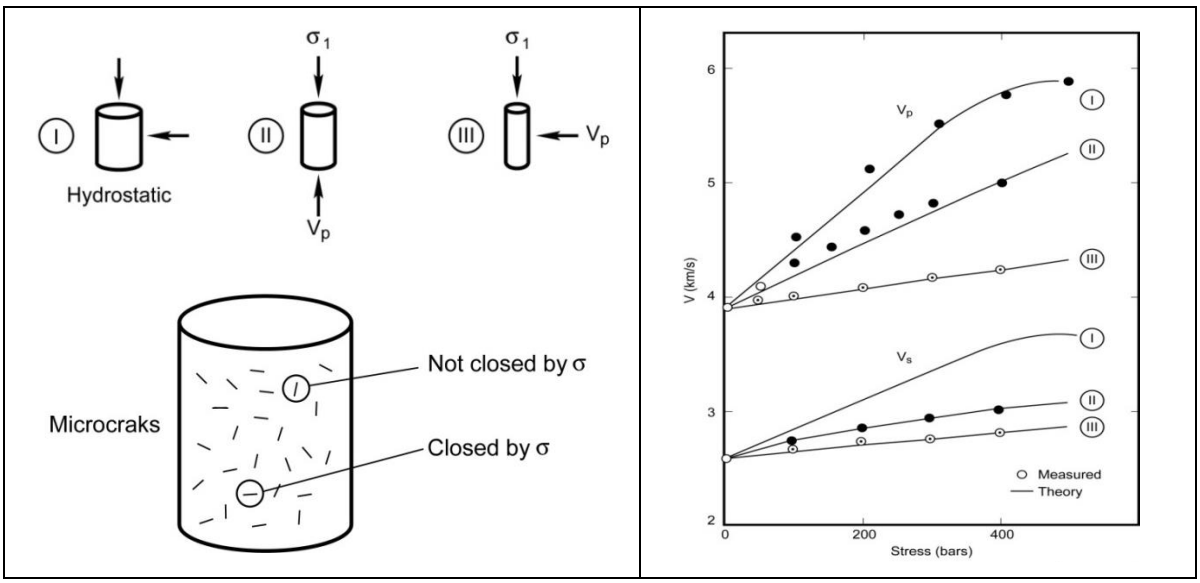

Fig 13 Microcrack behaviour under stress, showing that equal all-round (hydrostatic) stress has the most 'positive' effect on velocity, while V_P measured perpendicular to principal (axial) stress has least effect due to micro-cracks remaining open parallel to stress application. (Nur, 1971)

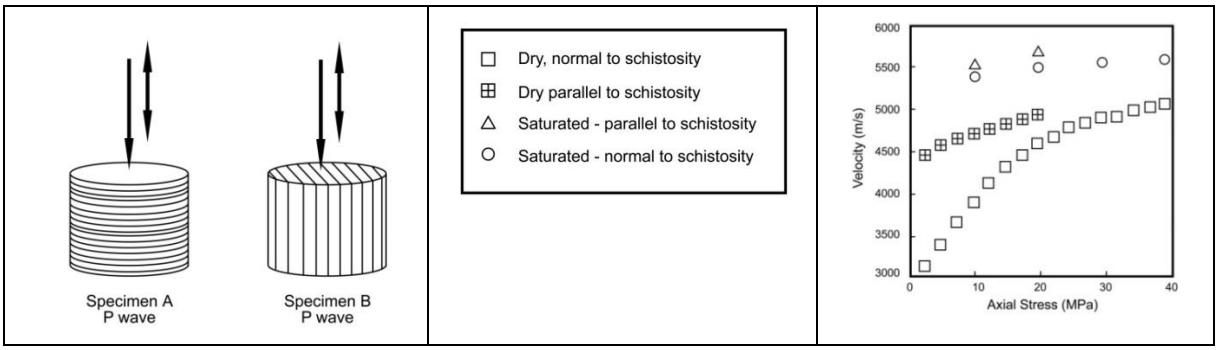

Fig 14 Effect of schistocity on velocity anisotropy in gneiss, loaded up to 40MPa, parallel or perpendicular to the fabric. Hesler et al., 1996. Note the strong influence of 'dryness' in lowering the velocity at low stress

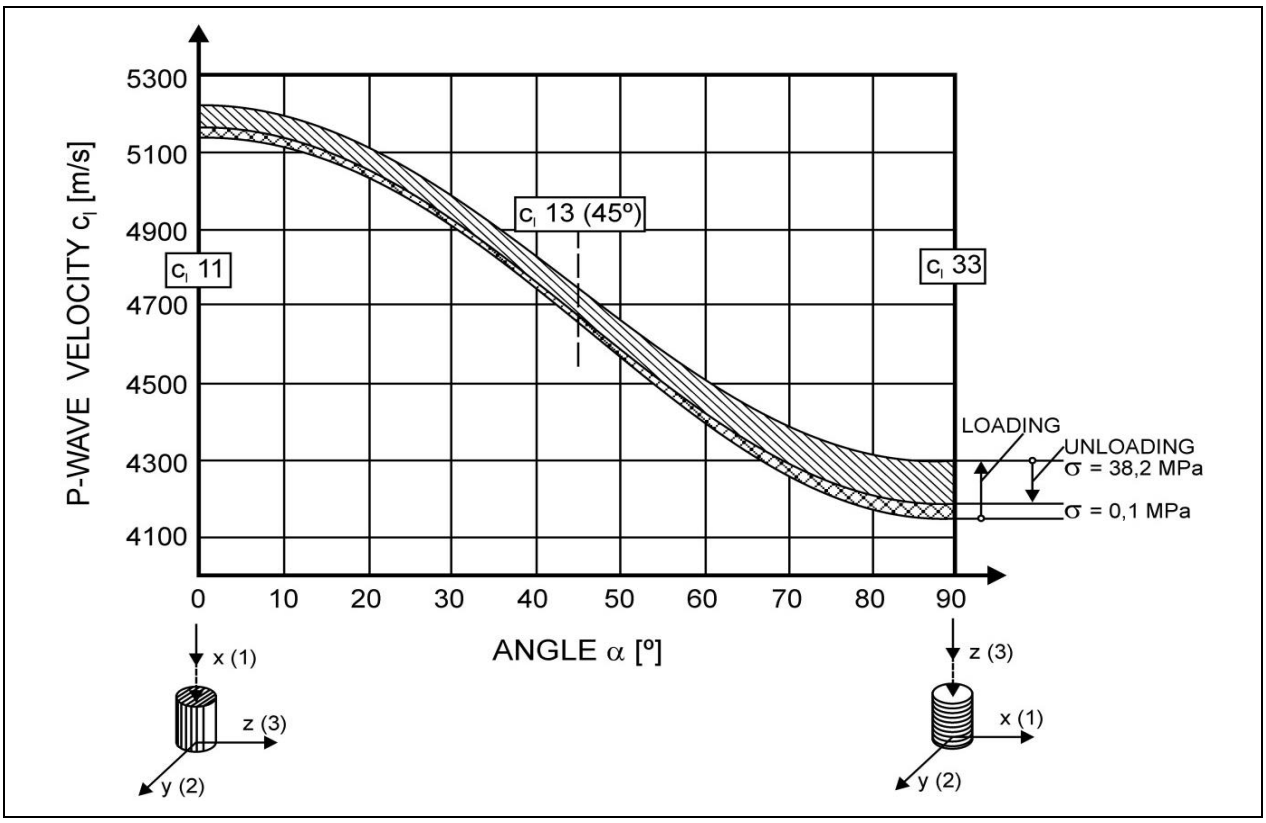

Fig 15 Intact samples of slate, both when loaded and (almost) unloaded, demonstrate a smooth variation of velocity with incident angle. (Duellmann and Heitfeld, 1978)

When the rock mass instead of the rock matrix has a much larger-scale 'fabric' due to inter-bedding, the velocity anisotropy naturally applies to the less frequent larger-scale inter-beds. In the case shown in Figure 16 it is the inter-bedded marl and sandstone which demonstrate differentiated velocity, expressed as V_P^2, and deformation modulus (back-calculated from MPBX measurements beneath plate-loading locations). In addition these dual measurements demonstrate an EDZ surrounding the dam investigation adit, with an additional effect of more loosening (lower V_P and lower E_{mass}) in the presumably unsupported invert (see D_1 and D_2).

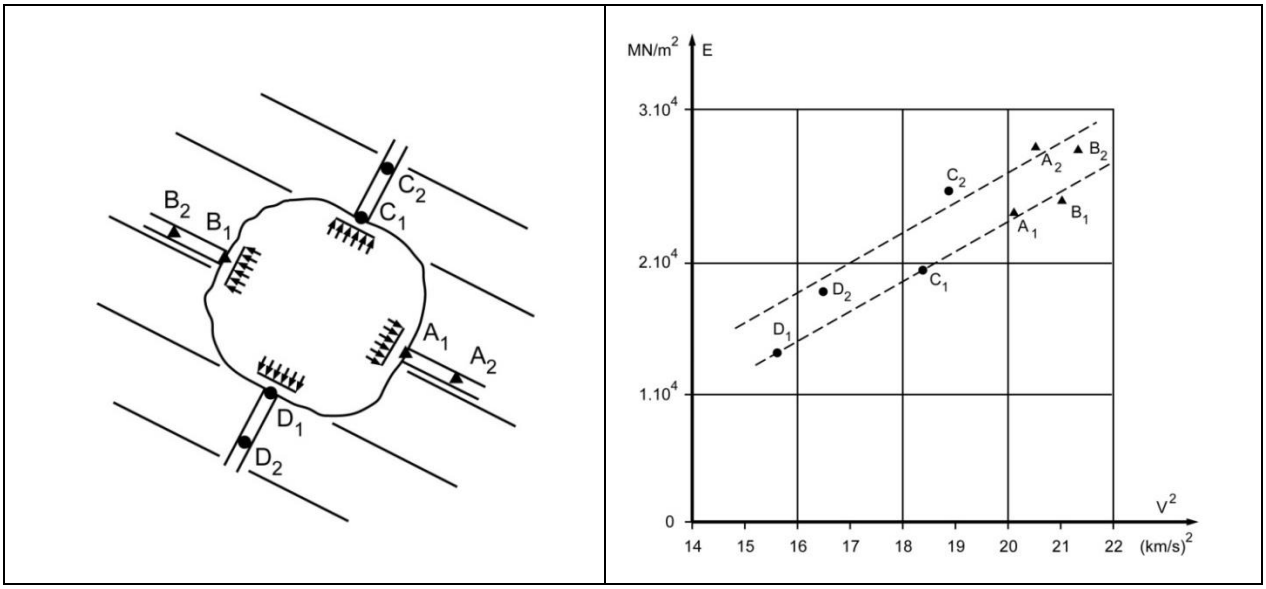

Fig 16 Anisotropy due to marl/sandstone inter-beds. 'Correlated' effects on Vp and Emass, and indications

of the effect of excavation disturbance. (Oberti et al., 1979)

Progressing onwards to the scale of hundreds of meters and a jointed rock mass, we see in Figure 17 the evidence from VSP (vertical seismic profiling) of anisotropically distributed jointing and/or the effect of horizontal stress anisotropy on the jointing. Both the jointing in the uppermost 300m and the jointing in the 460-520m depth interval show semi-consistent azimuthal anisotropy. A further effect shown is higher velocity at greated depth (1.5 to 2.0 km/s higher). This of course might be influenced by a change of rock type (harder, lower porosity) or less frequent jointing at greater depth, signifying higher deformation modulus, and higher Q-values.

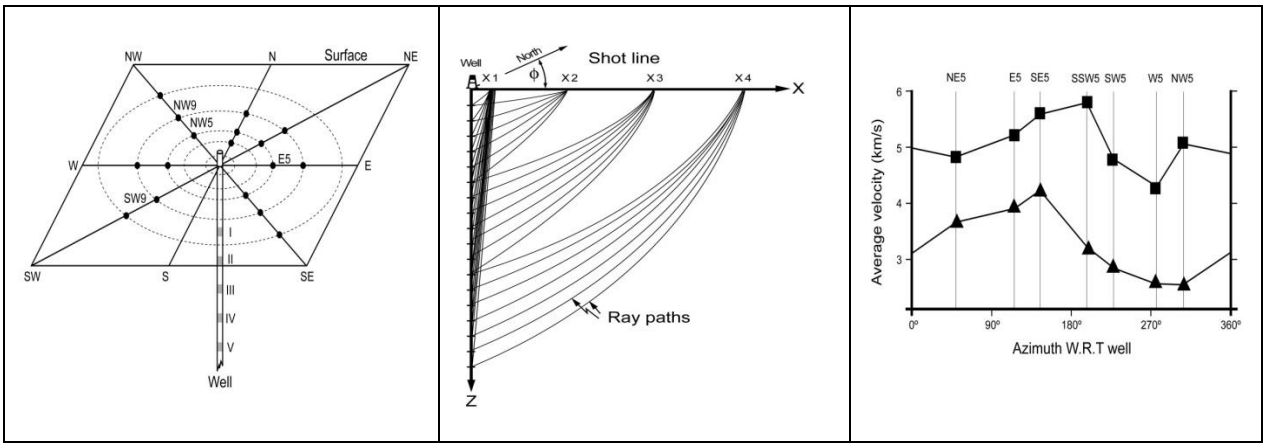

Fig 17 VSP with multı-azımuth shot poınts, shows Vp (mean) for 460-520m (top) and 0 to 300m depth ranges. A strong effect of depth causing higher velocity can be noted, but the azimuthal anisotropy remainsally strong. Presumably the rock mass surrounding the well has dominant jointing and/or stress-induced anisotropy. (Leary and Henyey, 1985)

Indirect evidence for anisotropy at reservoir scale is given by observations of the most productive pairs of injecting and producing wells, in water-flood operations. Heffer (2002) collected the numerous cases shown in Figure 18 that suggest a dominance of stress-oriented features, but with a significant population of 'conjugate' events, suggesting that shearing can also be involved (indeed needs to be involved) for improved production. If the joint or fracture set involved is without shear displacement, unlike the case illustrated in Figure 19, then the possibility of closure by the minimum stress, as discussed and modelled by Barton, 2006 has to be considered as a distinct possibility if not probability.

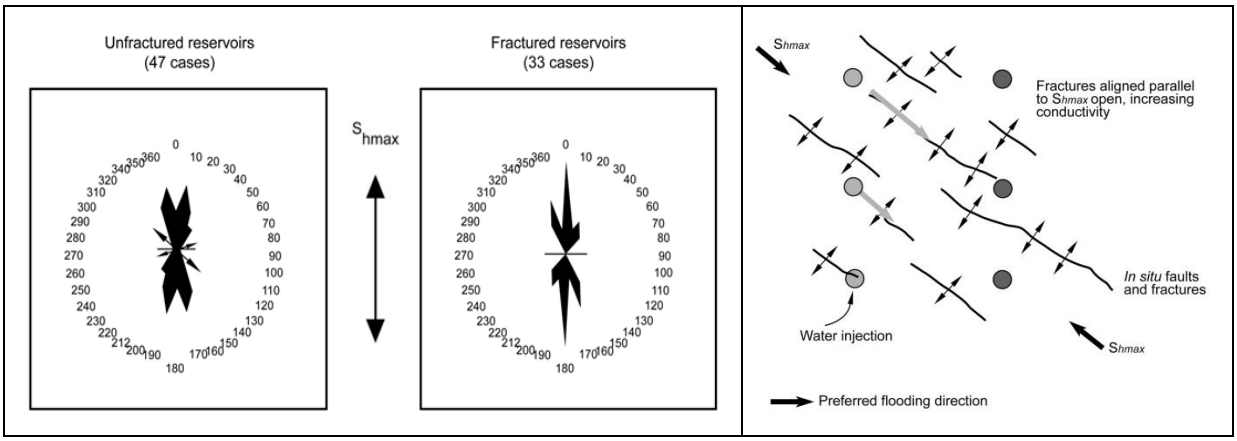

Fig 18 a, b and c. Left and centre: Conducting fractures in oil reservoirs represented as single or conjugate sets, tend to align with major principal stress (Heffer, 2002). The right-hand figure, not involving shearing, represents the traditional geophysics thinking. It can be a viable model if the fracture set involved is minerally 'frozen' in the form of channels which resist closure by the minimum principle stress. Each of the above illustrations are indications of strong anisotropic permeability

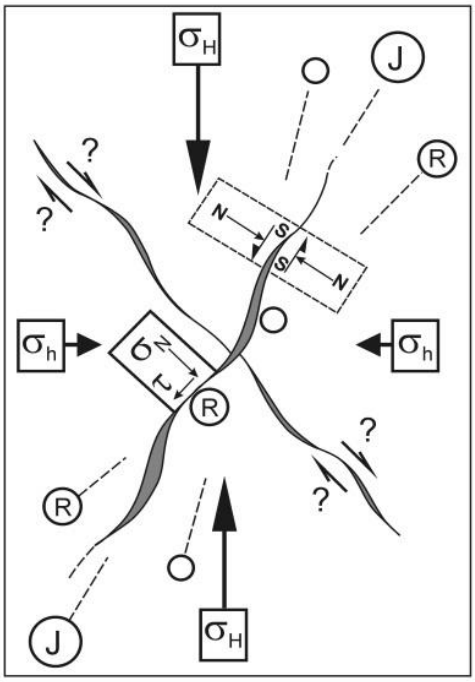

Fig 19 As emphasised in Barton, 2006, there is generally a dominant joint set, which will tend to rotate the principal permeability direction away for the principal stress direction if some shearing is involved. This tendency is presumably seen in both of Heffer's diagrams in Figure 18a and b

A small-scale 'demonstration' of conjugate behaviour is shown in Figure 20. An idealized '1x1 m' window looking into a representative porous and jointed (fractured) part of the compacting Ekofisk reservoir is shown. The one-dimensional (roller-boundaries) shown on the left, constrain the 2D representation of reservoir fracturing (jointing) to 1D compaction. The compaction and joint (or fracture) shearing can occur because a modelled 20 MPa reduction in oil pressure increases the effective stress so much that pore collapse occurs, thereby making space for down-dip shearing and almost maintenance of permeability. Shear strength is highly non-linear.

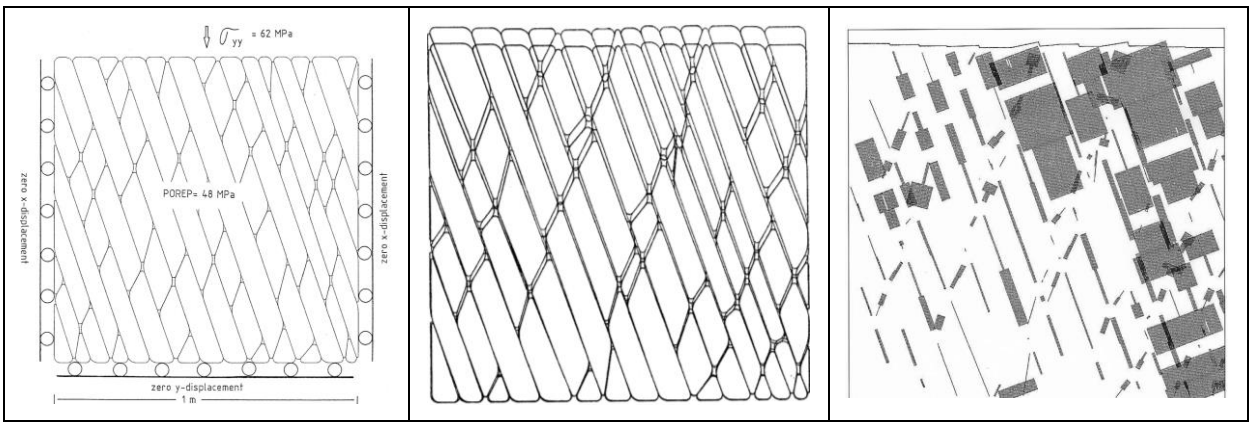

Fig 20 a, b and c A dominant joint set which shears during compaction and production more than the secondary set, creates local anisotropy and would deviate the fast shear wave axis. The mechanism helps to maintain some production (i.e. permeability) despite the compaction, by allowing more easy transport of petroleum from the compacting matrix. It is interesting to note that slickensides were seen in core from water-flood holes, but not in the exploration holes of the late nineteen sixties. Barton et al. (1988).

This section on seismic anisotropy (and coupled permeability effects) would be incomplete without mention of shear wave polarization into fast and slow axes as a result of the presence of an assumed set of aligned fractures at reservoir depth. The geophysics interpretation is traditionally that there is one set of principal stress-aligned fractures (some even believe it to be due to stress-aligned microcracks). Figure 21a from Schlumberger authors and collaborators shows the assumed single set of stress-aligned fractures as the presumed cause of fast and slow

axes (Barkved et al., 2004). The same stress-oriented ‘model’ is assumed by Horn (2003) in Figure 21b.

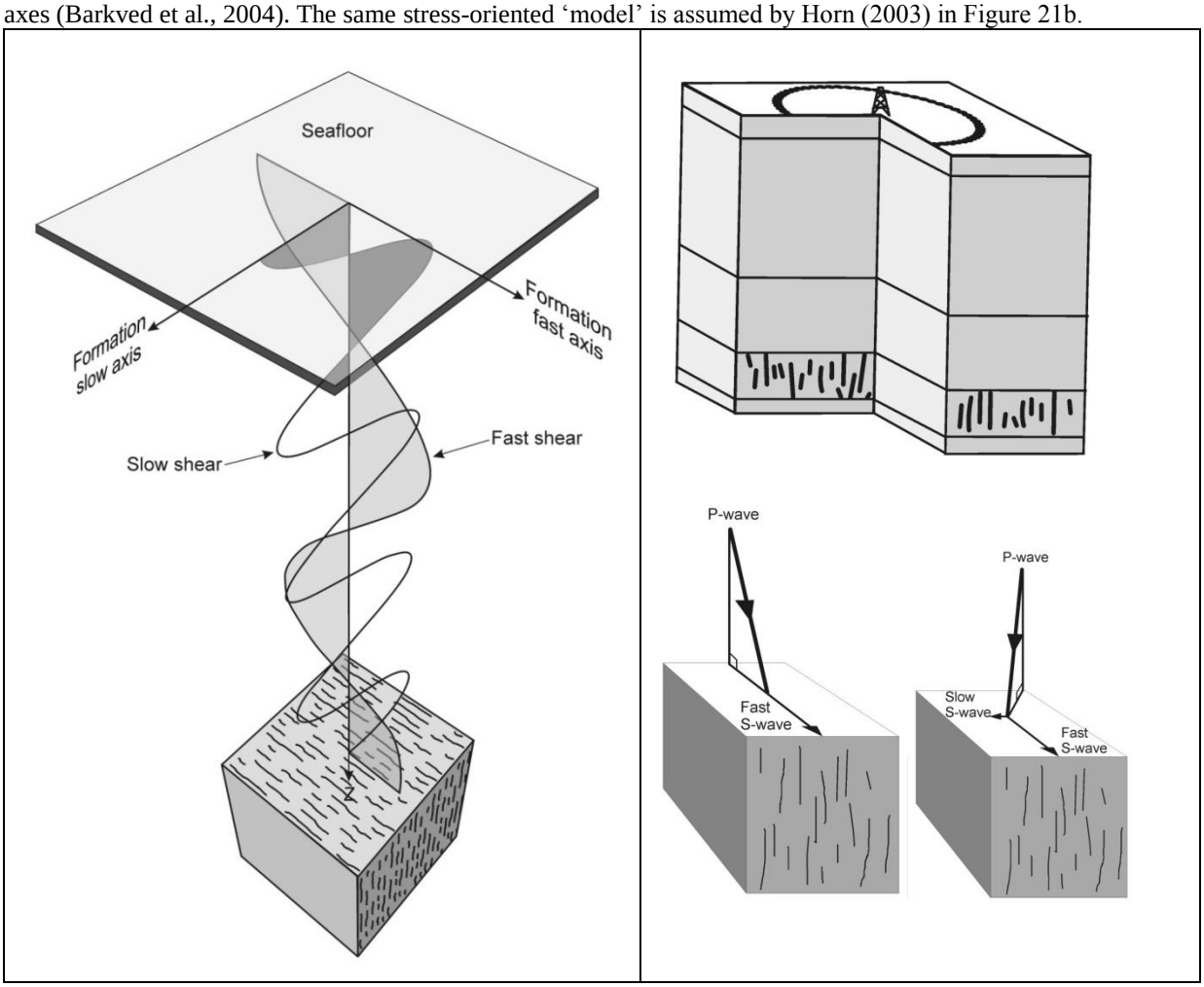

Fıg 21 Shear wave polarization concept as vizualized by geophysicists. Both sets of authors (Barkved et al., 2004 and Horn 2003) assume that one set of stress-aligned fractures (or even micro-cracks) are responsible for the polarization. In Barton, 2006 it is argued that one set does not constitute a very viable fractured reservoir, so shearing of conjugate sets is preferred. This would also show some stress alignment.

8 TUNNELS AND WELLBORES IN HIGHLY ANISOTROPIC STRESS FIELDS

To almost end this pictorial introduction to anisotropy, we will briefly describe a very interesting case of stress anisotropy experienced at the 1450 Mw Ita hydroelectric project in SE Brazil. The effect of the high horizontal stress in the region was accentuated by a bend in the river causing a steep ridge, across which the project was constructed. The distinctive ridge is seen in the satellite photo in Figure 22a, and in the two site photographs taken during and after construction (Figures 22 b and c). A total of ten tunnels crossed this ridge (five diversion tunnels, and five inclined pressure tunnels). In addition to the regional stress concentrated in the ridge separating the river meander (approx.11 km long), there was the influence of basalt flows with quite high Q-values sandwiched between basalt flows with quite low Q-values.

These flows of different stiffness were assumed to cause significant contrasts in deformation moduli, thereby attracting even higher horizontal stresses in the stiffest layers. All tunnels suffered stress-induced fracturing of one sort or another. A K_0 as large as 20-25 was interpreted from the extreme behaviour, which was unexpected at 50-75 m depth in UCS ≈ 200 MPa rock.Table 1 shows some of the assumed magnitudes of stress anisotropy, stress/strength ratios, SRF, and depth of failure at Ita HEP. The exceptionally large diversion tunnels of approximately 16 m span and up to 18 m height were severely compromised by the stress fracturing, causing large-scale ‘break-out’ (Figure 23) which was from 3 to 4 m deep in the arch and even more extreme in the invert, due to occasional high-velocity eroding flood flows.

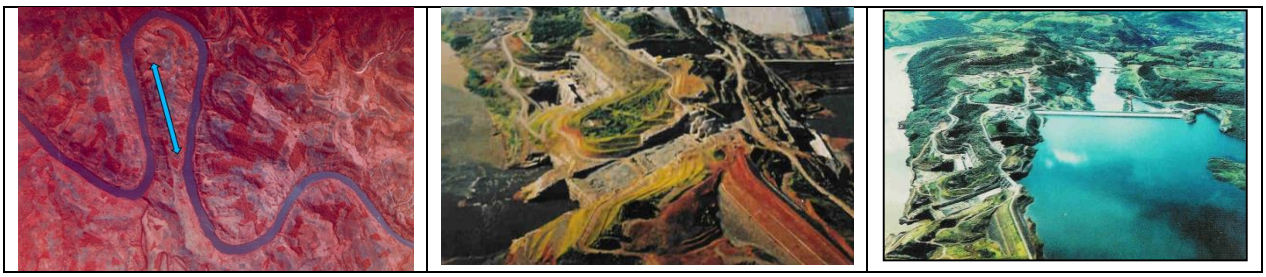

Figure 22 The 1,450 Mw Ita hydroelectric project in SE Brazil was constructed across the narrow stress-concentrating ridge formed by the 11 km long river meander. A major dyke is marked by the blue arrow, signifying a historic major principal stress. Five diversion tunnels suffered stress-induced fracturing and '12 o'clock' and '6 o'clock' over-break of 2 to 4m depth. The five pressure tunnel *linings* suffered tensile cracking across their 9 o'clock and 3 o'clock diameters, which was repaired with epoxy treatment. The emergency spillway was also severely cracked in the NNW-SSE direction. Barton and Infanti (2004).

Table 1 Some of the extreme stress levels and stress/strength ratios back-calculted from Ita HEP rock failure phenomena.

Ita HEP, Brazil: $\sigma_H \approx 40$ MPa, $\sigma_V \approx 1.5$ MPa at 50m depth (!)
$\sigma_\theta / \sigma_c \approx 115/200 \approx 0.6$ SRF $\approx$ 25 to 35
depth of failure / 'radius' (D_f /a) $\approx$ (3+7m)/7m $\approx$1.4
(see $\sigma_{max} / \sigma_c \approx 0.6$) in Figure 23

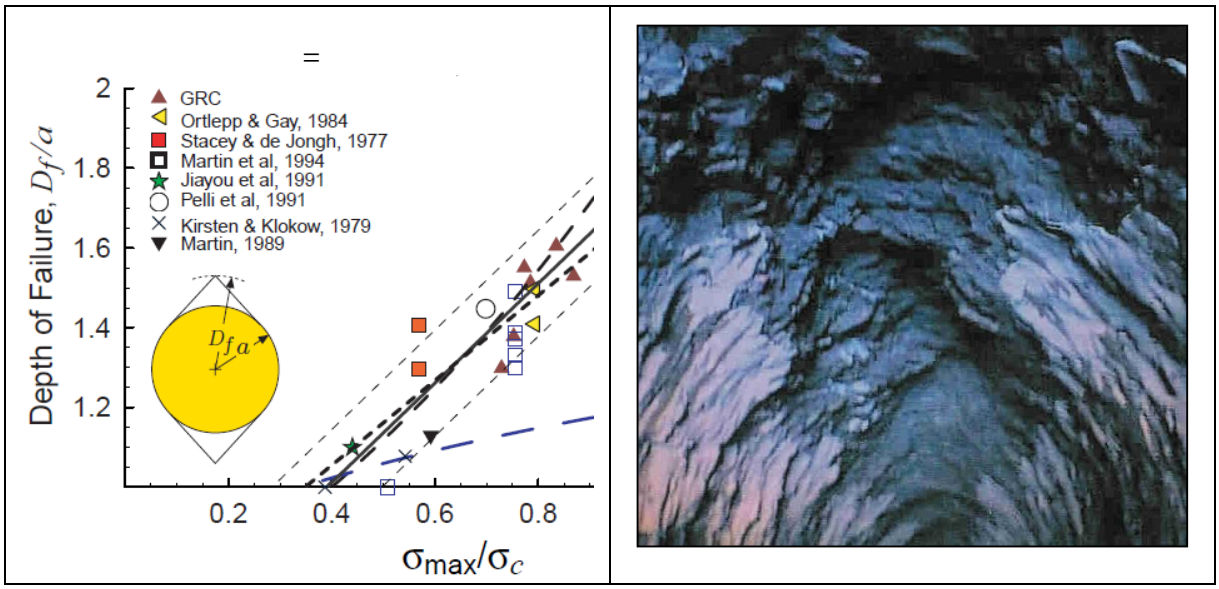

Fig 23 Depth of failure D_f/a estimation for the 16 x 18m diversion tunnels at Ita HEP. The initiation of stress fracturing shown in the left-hand diagram, from Martin et al. (2001) mostly from mining experiences, occurs at the same stress/strength ratio (≈ 0.4) in deep transport tunnels, and was reflected in rapidly increasing SRF (stress reduction facors) in the Q-system rating tables of Barton and Grimstad (1994).

The extreme stress anisotropy and extreme break-out illustrated in the Ita hydroelectric project represents a large-scale vision of what petroleum geomechanics engineers are measuring with caliper logs down wellbores, in order to estimate the direction and magnitude of horizontal stress anisotropy. Drill-cuttings of different size give clues about how strong the breakout is, and the acoustic well logs can be analysed for the 'angular extent' of the break-out, and may also give evidence of tensile failure across the perpendicular diameter, due to the respectively positive and potentially negative tangential stress concentrations.

Based on assumptions of continuity (which of course breaks down when actual failure is ocurring), the maximum and minimum tangential stress concentrations are as follows: $\sigma_{\theta\ max} = 3\sigma_1 - \sigma_3$ (this may cause 'dog-earing' or over-break), and $\sigma_{\theta\ min} = \sigma_1 - 3\sigma_3$ (this may cause tensile failure across the diameter at right-angles to that where the break-out has occurred).

It is not possible to see (optically) inside the wellbores nor *inside the walls* of the wellbores where such anisotropic-stress phenomena are ocurring. Nevertheless, by employing physical or numerical models, some ideas of the phenomena of 'dog-earing' due to stress-induced fracturing can be obtained. Figure 24 shows images of drilling and stress- induced log-spiral failure surfaces, which were always obtained when drilling in different directions into three-dimensionally loaded 50 x 50 x 50 cm cubes of uniformly cemented-sand model material (UCS ≈ 0.5 MPa). The log-spiral shear failure surfaces (with recorded shear deformation by coloured marker) ocurred in the case of the isotropic-material models. In the case of the layered already anisotropic 'rock mass', a plastic bending/buckling was induced.

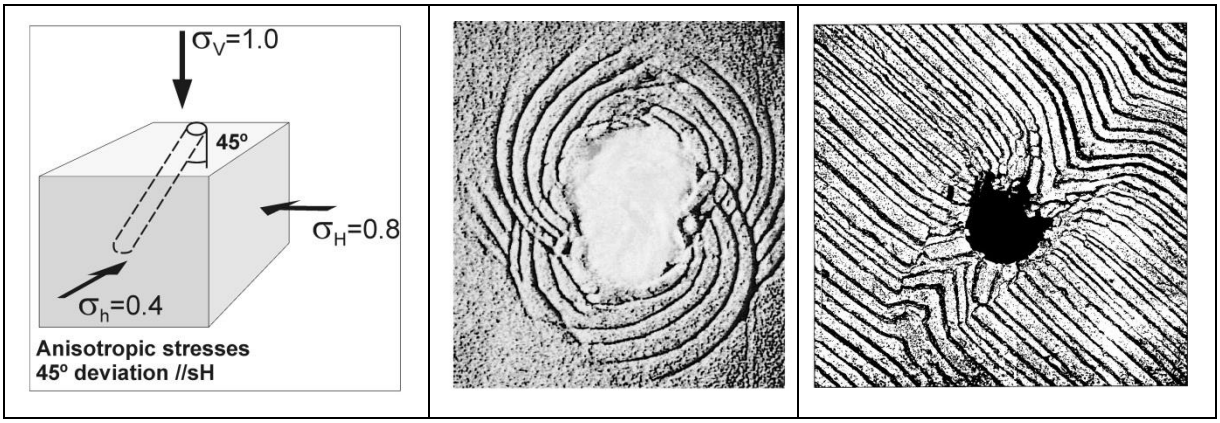

Fig 24 a, b and c Principal stress application in relation to direction of 45° deviated drilling parallel to σ_H direction. The anisotropic layered model, created by Bandis while working on our NGI project in the late nineteen eighties, showed classic bending/buckling tendencies with large deformation. See Addis et al. 1990.

9 ANISOTROPIC RQD, Q AND MODELLING NEEDS

When we compare a continuum model and a distinct element (discontinuum) model as in Figure 25, it is clear that in one case (only), we can represent an anisotropic structure, and learn of some interesting potential behaviour. For instance we see non-vertical deformation as a result of the dipping dominant joint set, when large-span 'motorway tunnels' are excavated in the stressed models. There is also an indication of a wedge fall-out in the left wall of one of the tunnels. If one 'drilled a borehole' in either model the equivalent RQD and Q values (using imagination of the third dimension) would be entirely different. Furthermore the RQD would be direction dependent, potentially showing high values if 'drilled' parallel to the dominant jointing (a poor sampling strategy), and lower RQD values if 'drilled' perpendicular to the dominant joint set in the case of Figure 25b.

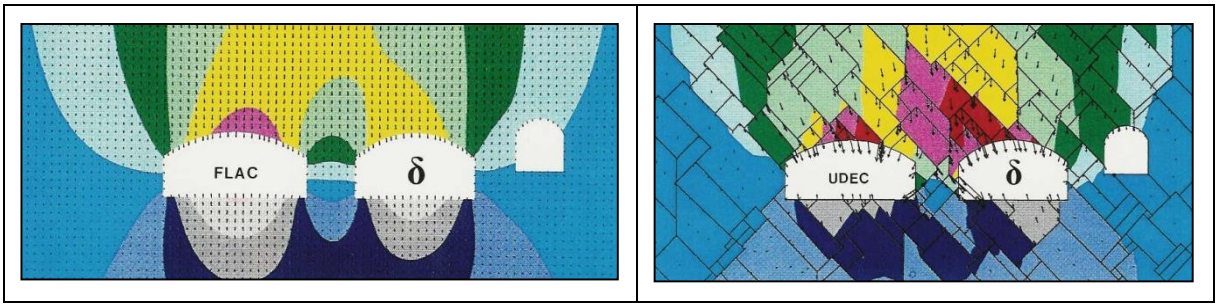

Fig 25 a and b Contrasting isotropic and anisotropic behaviour, as modelled by FLAC and UDEC-BB. (Models by Lise Backer, NGI, priv. comm. 1995).

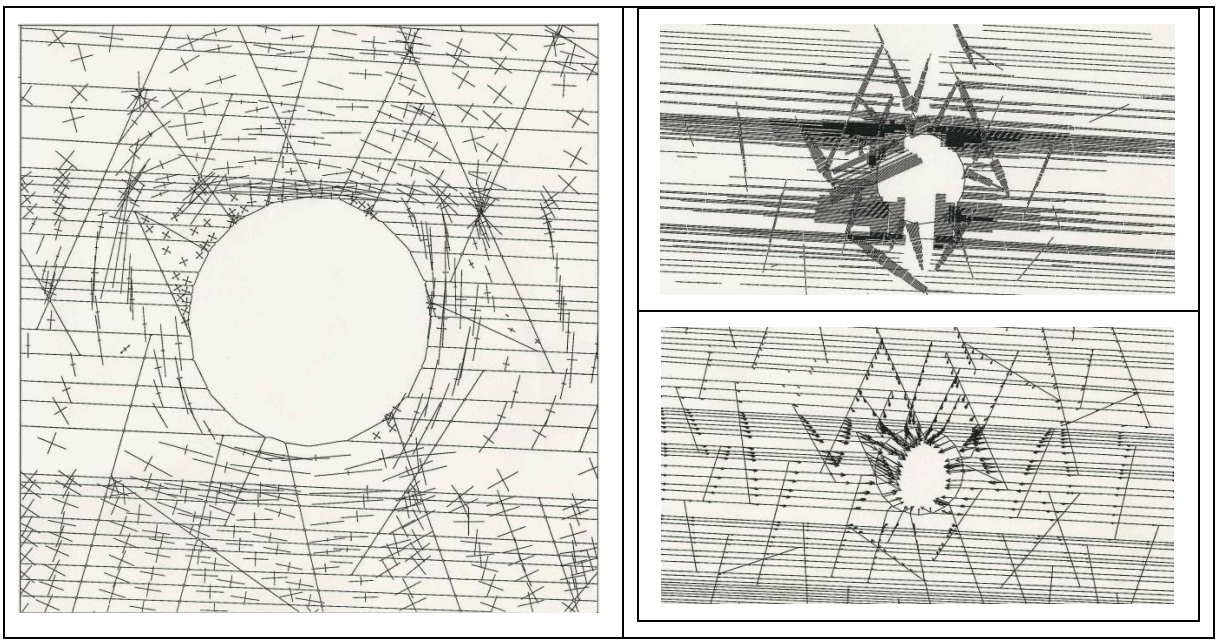

Fig 26 A more anisotropic (St. Bee's sandstone) UDEC-BB model from the Sellafield nuclear waste isolation project. Sedimentary layering, and anisotropic stress acting together, give an additional source of anisotropy, especially the shearing (top-right) as a result of spiral-access TBM 'excavation'.The first author was project manager for these NGI studies in the early nineties. Barton, 2000.

If we again use our imagination of the third dimension and 'drill' core from the modelled 'rock mass' in Figure 26, it is very clear that the direction of 'drilling' will be fundamental for the RQD value (directional) and for the Q-value (also directional) resulting from e.g. vertical or horizontal sampling. All properties linked to Q-values will also be anisotropic, for instance velocity and deformation modulus and permeability.

10 CONCLUSIONS

1. Anisotropy is so common that a specialist conference on isotropic behaviour would be a viable alternative, if participants were to describe the rare instances of actual isotropic behaviour, as opposed to the assumed isotropic behaviour. Naturally the findings from such a conference would not be very enlightening.

2. Anisotropic behaviour is so widespread because of the combined effects of anisotropic structure, most typically in the form of bedding, and because of anisotropic stress in the past, which has caused the formation of distinctive joint sets.

3. Anisotropic behaviour is most marked in the case of permeability (orders of magnitude), but important azimuthal variation in veliocity and deformability are noted, with most effect when measuring or modelling properties parallel or perpendicular to sedimentary and metamorphic structures, such as bedding, schistocity, and cleavage.

11 REFERENCES

Addis, M.A., Barton, N., Bandis, S.C. & Henry, J.P. 1990. Laboratory studies on the stability of vertical and deviated boreholes. 65th Annual Technical Conference and Exhibition of the Society of Petroleum Engineers, New Orleans, September 23-26, 1990.

Bandis, S., Lumsden, A. & Barton, N. 1981. Experimental studies of scale effects on the shear behaviour of rock joints. *Int. J. of Rock Mech. Min. Sci. and Geomech. Abstr*. 18, 1-21.

Bandis, S., Lumsden, A.C. & Barton, N. (1983). Fundamentals of rock joint deformation. *Int. J. Rock Mech. Min. Sci. and Geomech. Abstr.* Vol. 20: 6: 249-268.

Barkved, O., Bartman, B., Gaiser, J., Van Dok, R., Johns, T., Kristiansen, P., Probert, T. & Thompson, M. 2004. The many facets of multicomponent seismic data. *Oilfield Rev*., *Summer 2004*, 42–56, Schlumberger.

Barton, N. (1973). Review of a new shear strength criterion for rock joints, *Engineering Geology*, Elsevier, Amsterdam, Vol. 7, pp. 287-332.

Barton, N. (1981). Hydraulic fracturing to estimate minimum stress and rockmass stability at a pumped hydro project. Proc. of *Workshop on Hydraulic Fracturing Stress Measurements*, Monterey, USA.

Barton, N. (1986). Deformation phenomena in jointed rock. 8th Laurits Bjerrum Memorial Lecture, Oslo. *Geotechnique*, Vol. 36: 2: p.147-167.

Barton, N., Makurat, A., Hårvik, L., Vik, G., Bandis, S., Christianson, M. & Addis, A. 1988. The discontinuum approach to compaction and subsidence modelling as applied to Ekofisk. BOSS '88. Proc. of Int. Conf. on Behaviour of Offshore Structures, Trondheim. Vol. 1: 129-141.

Barton, N. & Grimstad, E. 1994. The Q-system following twenty years of application in NMT support selection. 43rd Geomechanic Colloquy, Salzburg. Felsbau, 6/94. pp. 428-436.

Barton, N. 1994. A Q-system case record of cavern design in faulted rock. 5th Int. Rock Mechanics and Rock Engineering Conf., Tunnelling in difficult conditions, Torino, Italy, pp. 16.1-16.14.

Barton, N. 2000. *TBM Tunnelling in Jointed and Faulted Rock*. 173p. Balkema, Rotterdam.

Barton, N. & Infanti, N. 2004. Unexpected stress problems in shallow basalts at the Ita hydroelectric power project in S.E. Brazil. Proc. ARMS 2004 : 3rd Asian Rock Mechanics Symposium, Kyoto.

Barton, N. 2006. *Rock Quality, Seismic Velocity, Attenuation and Anisotropy.* Taylor & Francis, UK & Netherlands, 729 p.

Barton. N. 2010. Low Stress and High Stress Phenomena in Basalt Flows. Keynote paper. *3rd International Workshop on Rock Mechanics and Geo-Engineering in Volcanic Environments.* Tenerife.

Duellmann, H. & Heitfeld, K.H. 1978. Influence of grain fabric anisotropy on the elastic properties of rocks. *Proc. 3rd IAEG Congress*, Madrid. *II*(*1*): 150–162. Madrid: Imprime ADOSA.

Heffer, K. 2002. Geomechanical influences in water injection projects: an overview. *Oil Gas Sci.Tech. Rev. IFP*, *57*(*5*): 415–422.

Hesler, G.J., Cook, N.G.W. & Myer, L. 1996. Estimation of intrinsic and effective elastic properties of cracked media from seismic testing. *2nd NARMS '96.* Montréal, Québec. Aubertin, Hassani & Mitri (eds.). *1*: 467–473. Rotterdam: Balkema.

Horne, S. 2003. Fracture characterization from walkaround VSPs. *Geophys. Prospect.*, *51*: 493–499.

King, M.S., Myer, L.R. & Rezowalli, J.J. 1984. Cross-hole acoustic measurements in basalt. *25th US Symp. on Rock Mechanics*,Evanston, IL. Dowding & Singh (eds.). New York: Society of Mining Engineers, 1053–1061.

Leary, P.C. & Henyey, T.L. 1985. Anisotropy and fracture zones about a geothermal well from *P*-wave velocity profiles. *Geophysics*, *50*(*1*): 25–36.

Martin, D.C., R. Christiansson and J. Soderhall. 2001. Rock stability considerations for siting and constructing a KBS-3 repository, based on experience from Äspö HRL, AECL's HRL, tunnelling and mining. *SKB (Swedish Nuclear Fuel Co.)* Stockholm, TR-01-38, 2001.

Nur, A. 1971. Effects of stress on velocity anisotropy in rocks with cracks. *J. Geoph. Res.*, *76*(*8*): 2022–2034.

Oberti, G., Carabelli, E., Goffi, L. & Rossi, P.P. 1979. Study of an orthotropic rock mass: Experimental techniques, comparative analysis of results. *Proc. 4th ISRM Congress*, Montreux, *2*: 485–491. Rotterdam: Balkema.

Quadros, E. & Correa Filho, D. (1993). Scale effects on the hydraulic properties determined by *in situ* 3-D tests. *ISRM Int. Symp. on Rock Mechanics*, EUROCK´ 93 – Scale Effects in Rock Masses, Lisbon. Rotterdam: Balkema, 1993. v. 1. p. 313-321.

Quadros, E. & Correa Filho, D. (1999). 3-D hydraulic tests for the subway of São Paulo, Brazil. *Proc. 9th ISRM Congress on Rock Mechanics*, Paris. Rotterdam: Balkema, 1999. v. 2. p. 817-823.

Quadros, E. & Abrahão, R. (2002). Percolation and grouting in basaltic rocks – some Brazilian experience. Proc. *ISRM Int. Symp. on Rock Mechanics*, EUROCK´ 2002 – *Workshop on Volcanic Rocks*. Madeira, Portugal. Ed. SPG: v.1 p. 125-135.

Quadros, E. & Correa Filho, D. (1998). Analysis of grouting efficiency and deformations using three-dimensional hydraulic tests. *Vth South American Rock Mech Cong., ISRM Regional Symp. SAROCK´S 98, Brazil. Ed. Politécnica, EDUSP, v.1. p.515-523.*

Nomenclature

BB	Barton-Bandis constitutive model for rock joints
E_{mass}	static modulus of deformation
E	average physical aperture of a joint
e	hydraulic aperture of a joint
EDZ	excavation disturbed zone
FLAC	two-dimensional continuum code for modelling small or large deformations in rock or soil
J_a	rating for joint alteration, discontinuity filling
JCS	joint wall compression strength
J_n	rating for number of joint sets
J_r	rating for joint surface roughness
JRC	joint roughness coefficient
J_w	rating for water softening, inflow and pressure effects
K	permeability (units m/s)
Kn	normal stiffness of a joint
Ks	shear stiffness of a joint
K_{int}	intermediate principal permeability
K_{max}	maximum principal permeability
K_{min}	minimum principal permeability
k_o	ratio of σ_h/σ_v
NGI	Norwegian Geotechnical Institute
Q	rock mass quality rating (range 10^{-3} to 10^3)
Q_c	rock mass quality rating (Q, or Q_o normalized by σ_c /100)
Q_o	Q calculated with RQD_o oriented in the loading or measurement direction
Q_{seis}	seismic quality factor – the inverse of attenuation (used by geophysicists, normally with the P- and S-wave components 'Q_p' and 'Q_s')
RQD	rock quality designation (% of core ≥ 10 cm in length)
RQD_o	RQD oriented in the loading or measurement direction (in the Q_{TBM} model it is in the tunnelling direction)
σ_c	uniaxial strength
σ_v	vertical (principal) stress
σ_h	horizontal (principal) stress
σ_θ	tangential stress (surrounding an excavation, borehole)
UDEC	universal distinct element code, for modelling a two-dimensional, 1m thick slice of the rock mass
V_p	P-wave seismic velocity (km/s)
V_s	S-wave seismic velocity (km/s)